The Canadian Mineralogist
Vol. 39, pp. 1653-1663 (2001)

THE CRYSTAL STRUCTURE OF (001) TWINNED XILINGOLITE, $Pb_3Bi_2S_6$, FROM MITTAL–HOHTENN, VALAIS, SWITZERLAND

PETER BERLEPSCH[§] AND THOMAS ARMBRUSTER

Laboratorium für chemische und mineralogische Kristallographie, Universität Bern, Freiestrasse 3, CH-3012 Bern, Switzerland

EMIL MAKOVICKY

Geological Institute, University of Copenhagen, Øster Voldgade 10, DK-1350 Copenhagen K, Denmark

CLIVIA HEJNY

Laboratorium für chemische und mineralogische Kristallographie, Universität Bern, Freiestrasse 3, CH-3012 Bern, Switzerland

DAN TOPA

Departement für Geologie und Mineralogie, Universität Salzburg, Hellbrunner Strasse 34/III, A-5020 Salzburg, Austria

STEFAN GRAESER

Mineralogisch-Petrographisches Institut, Universität Basel, Bernoullistrasse 30, CH-4056 Basel, Switzerland

ABSTRACT

The crystal structure of xilingolite, ideally $Pb_3Bi_2S_6$, space group $C2/m$, $Z = 4$, a 13.511(3), b 4.0850(11), c 20.649(2) Å, β 92.15(2)°, was solved and refined from single-crystal X-ray data collected on (001) twinned crystals (R_1 = 8.65% for 1520 reflections with $I > 2\sigma_I$). Xilingolite is a $^{4,4}L$ homologue of the lillianite homologous series. Its crystal structure and chemical composition are similar to those of lillianite, but this mineral has increased Pb–Bi order and reduced symmetry compared to lillianite, and thus is a dimorph of $Pb_3Bi_2S_6$. In lillianite and xilingolite, alternating layers of PbS archetypes, cut parallel to $(311)_{PbS}$, are linked by trigonal PbS_6 prisms. In lillianite, this prism is bicapped, PbS_{6+2}, but in xilingolite, the prism is only monocapped, PbS_{6+1}. This difference in coordination gives rise to underbonding of one S site in xilingolite, balanced by an ordered arrangement of Bi^{3+} on an adjacent metal site. Electron-microprobe analyses yielded an empirical formula $Ag_{0.04(0)}Pb_{2.91(2)}Bi_{2.07(1)}S_{5.98(2)}$. Compared with the simplified formula $Pb_{3.18}Bi_{1.81}S_6$ given in the original description, the formula of the xilingolite from Mittal–Hohtenn, Valais, Switzerland contains less Pb and more Bi, giving a formula close to $Pb_3Bi_2S_6$ with integer stoichiometry, identical to the composition of lillianite.

Keywords: xilingolite, crystal structure, twinning, lillianite homologue, electron-microprobe analyses, cannizzarite, Bi-containing galena, Mittal–Hohtenn, Valais, Switzerland.

SOMMAIRE

Nous avons affiné la structure cristalline de la xilingolite, dont la composition idéale est $Pb_3Bi_2S_6$, groupe spatial $C2/m$, Z = 4, a 13.511(3), b 4.0850(11), c 20.649(2) Å, β 92.15(2)°, à partir de données en diffraction X déterminées sur cristal unique maclé sur (001) (R_1 = 8.65% pour 1520 réflexions observées ayant $I > 2\sigma_I$). La xilingolite est un homologue $^{4,4}L$ de la série de la lillianite. Sa structure et sa composition chimique ressemblent à celles de la lillianite, mais ce minéral est plus complètement ordonné dans sa distribution de Pb et Bi, et donc sa symétrie s'en trouve réduite. Il s'agit donc d'un dimorphe de $Pb_3Bi_2S_6$. Dans la lillianite aussi bien que la xilingolite, des couches en alternance de l'archetype PbS, parallèles à $(311)_{PbS}$, sont liées par des prismes trigonaux PbS_6. Dans la lillianite, de tels prismes sont biterminés, PbS_{6+2}, mais dans la xilingolite, les prismes ne sont que monoterminés, PbS_{6+1}. Cette différence en coordinence mène à une déficience en valences de liaison à un site S dans la xilingolite,

§ *E-mail address*: peter.berlepsch@krist.unibe.ch

qui est accommodée par une mise en ordre des ions Bi^{3+} sur un site adjacent. Les analyses à la microsonde électronique ont donné une formule empirique $Ag_{0.04(0)}Pb_{2.91(2)}Bi_{2.07(1)}S_{5.98(2)}$. Comparée à la formule simplifiée proposée antérieurement pour l'échantillon holotype, $Pb_{3.18}Bi_{1.81}S_6$, la xilingolite de Mittal–Hohtenn, Valais, en Suisse contient davantage de Bi et moins de Pb, et sa formule se rapproche donc de $Pb_3Bi_2S_6$, avec une stoechiométrie intégrale et une composition identique à celle de la lillianite.

(Traduit par la Rédaction)

Mots-clés: xilingolite, structure cristalline, macle, homologue de la lillianite, données à la microsonde électronique, cannizzarite, galène bismuthifère, Mittal–Hohtenn, Valais, Suisse.

Introduction

Graeser (1984) reported on the assemblage of minerals found on dumps excavated during tunnel construction between Mittal and Hohtenn in Valais, Switzerland. Oxides, carbonates, tungstates, phosphates, silicates, and sulfides (simple and complex) were briefly described. Among the complex sulfides (or sulfosalts), cannizzarite $Pb_4Bi_6S_{13}$, cosalite $Pb_2Bi_2S_5$, heyrovskyite $Pb_6Bi_2S_9$, and two unknown minerals, M1 and M2, were found (Graeser 1984). Several years later, M1 was identified as galenobismutite, $PbBi_2S_4$, but the identity of M2 remained unknown. The powder pattern of M2 showed similarities with that of lillianite, $Pb_3Bi_2S_6$. Graeser (1984) thus concluded that the unknown mineral is probably also a Pb–Bi sulfosalt.

Recently, a yet unpublished work by the mineral collector H.-R. Rüegg about the ore and minerals from the lead mine Rotenberg, located near Goppenstein, in Valais, Switzerland, focused our attention on the unknown mineral M2. Subsequently, we obtained material from Graeser's original samples of M2 for further investigation. We have established that M2 is not a new mineral, but rather xilingolite, of simplified formula $Pb_3Bi_2S_6$, which was originally reported by Hong *et al.* (1982) from a skarn-type iron deposit in the Chaobuleng district, Xilingoa League, Inner Mongolia Autonomous Region, China. In the present paper, we describe the crystal structure of xilingolite from Mittal–Hohtenn on a modular basis and compare it to lillianite, with a focus on the differences in degree of cation order.

Review of the Literature

The lillianite homologous series (Makovicky & Karup-Møller 1977a, b), to which xilingolite belongs, is an accretionary series of mostly Pb–Bi–Ag sulfosalts, the structures of which consist of alternating layers of the PbS archetype, cut parallel to $(311)_{PbS}$. These planes also represent the reflection and contact planes of the unit-cell twinning. The overlapping octahedra of adjacent mirror-related layers are replaced by bicapped trigonal coordination prisms PbS_{6+2}, with the Pb atoms positioned on the mirror planes (Fig. 1).

Distinct homologues differ in the thickness of PbS-like layers. This thickness is conveniently expressed as the number *N* of octahedra in the chain of octahedra that runs diagonally across an individual archetype layer and is parallel to $[011]_{PbS}$ (Fig. 1). Each lillianite homologue can be denoted as ${}^{N1,N2}L$, where N_1 and N_2 are the (not necessarily equal) values of the two alternating sets of layers (Makovicky & Karup-Møller 1977a, b).

Sample Description

In the early 1980s, no geological or petrographic details about the Mittal–Hohtenn tunnel were available. From the geological map (Swiderski 1919), it became obvious that the tunnel cuts across paragneisses with intercalated amphibolites of the Aar massif, the Baltschieder granite, and Mesozoic sediments. Most of the known mineral samples originate from druses in the paragneisses, including those described in this paper.

Sulfosalts are found mainly in quartz druses, where they occur in more or less close association with galena. One exception is a sulfosalt, which we assumed to be heyrovskyite, but which turned out to be an oriented, submicroscopic intergrowth of distinct lillianite-related phases, denoted "lillianite" below, which grew as isolated crystals in a chlorite matrix in the paragneiss. Galena from Mittal–Hohtenn forms octahedra with an unusual but typical octahedral cleavage. This habit is commonly related to increased Bi contents in PbS (Graeser 1971). Owing to their typical habits and modes of association with galena, one can visually distinguish most of the sulfosalts so far reported from this locality: 1) Thin and deformed lamellae of cannizzarite grew directly on galena. 2) Hair-like fibers of cosalite are usually accompanied by galena, but did not grow on it. 3) The minute crystals of galenobismutite have been found in one sample only, and they overgrew galena (Graeser 1984). 4) Heyrovskyite is usually not intergrown with galena. The crystals are lath-like with a striation along the morphological elongation, and they usually are deformed. 5) Xilingolite and "lillianite" cannot be distinguished visually. They form crystals similarly striated as those of heyrovskyite, but with a more pronounced prismatic form (*i.e.*, they are not lath-like).

The fragments of xilingolite crystals were taken from one crystal that grew on galena (Fig. 2). This crystal has a bright silver color, metallic luster, and a prismatic form with striations parallel to the morphological elongation.

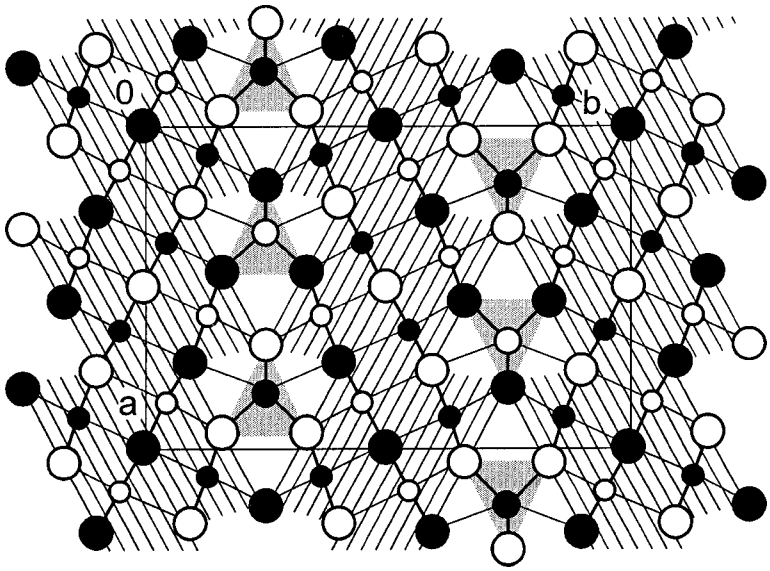

FIG. 1. The crystal structure of lillianite, $Pb_3Bi_2S_6$, an orthorhombic (*Bbmm* setting) $^{4,4}L$ homologue of the lillianite homologous series (Takagi & Takéuchi 1972). Circles, in order of decreasing size, denote S, Pb, (Pb,Bi). "PbS-like" layers are ruled, and bodies of bicapped trigonal coordination prisms of *M*3 (assumed Pb positions) are shaded. Void and filled circles indicate atoms at $z = 0.5$ and 0, respectively, along the 4 Å axis.

FIG. 2. Elongate and striated crystal of xilingolite, roughly 2 mm long, on galena showing an octahedral cleavage, together with quartz.

Chemical Analyses

Quantitative chemical analyses were performed on a JEOL JXA–8600 electron microprobe (EMP), controlled by a LINK–*eXL* system, operated at 25 kV, 35 nA, and with a counting time of 20 s for peaks and 7 s for background. The following standards and X-ray lines were used: $CuFeS_2$ (Cu*K*α, Fe*K*α), metallic Ag (Ag*L*α), CdTe (Cd*L*β, Te*L*α), Bi_2S_3 (Bi*L*α, S*K*α), PbS (Pb*L*α). The elements Cu, Fe, Sb, Cd, Te, and Se were found to be below the detection limits, except in "lillianite" (Sb: 0.08; Te 0.15 wt%), galena (Fe: 0.04; Te 0.08 wt%), and cannizzarite (Fe: 0.03; Te: 0.21 wt%). The raw data were corrected with the on-line ZAF–4 procedure; the results are listed in Table 1. The formula of xilingolite derived from the mean of seven EMP analyses is $Ag_{0.04(0)}Pb_{2.91(2)}Bi_{2.07(1)}S_{5.98(2)}$ or, in simplified form, $Pb_3Bi_2S_6$.

Compared with formulae given by Hong *et al.* (1982), either the simplified formula $Pb_{3.18}Bi_{1.81}S_6$ or the ideal one $Pb_{3+x}Bi_{2-2/3x}S_6$ (where $x = 0.3$), the formula of the xilingolite from Mittal–Hohtenn contains less Pb and more Bi, giving a formula close to $Pb_3Bi_2S_6$ with integer stoichiometry, identical to the composition of lillianite.

The galena from Mittal–Hohtenn contains up to about 1.1 wt% Bi and about 0.2 wt% Ag (Table 1). It is interesting to note that the proportion of Bi (0.62 at%) and Ag (0.21 at%) are not equal, thus the investigated galena contains more Bi than the matildite–galena substitution *sensu stricto* ($2\,Pb^{2+} \leftrightarrow Bi^{3+} + Ag^{+}$) would suggest (note: the substitution $3Pb^{2+} \leftrightarrow 2Bi^{3+} + \square$ can work as well, but the small number of analyses and the low contents of Bi and Ag do not allow us to draw a conclusion in this respect). The analyzed cannizzarite yielded a formula similar to those reported in literature. However, the sulfosalt assumed to be heyrovskyite has a composition similar to the analyzed xilingolite, but is richer in Ag and Bi and contains less Pb. The unit-cell determination did not allow us to decide between lillianite and xilingolite, thus the material is best described as an oriented, submicroscopic intergrowth of different lillianite-related phases, referred to here as "lillianite" for convenience.

TABLE 1. CHEMICAL COMPOSITION OF XILINGOLITE, "LILLIANITE", Bi-CONTAINING GALENA, AND CANNIZZARITE FROM MITTAL–HOHTENN, SWITZERLAND

	Ag	Pb	Bi	S	Sum
Xilingolite					
1	0.36	49.19	35.16	15.87	100.52
2	0.31	49.21	34.96	15.44	99.92
3	0.35	49.07	35.28	15.43	100.13
4	0.35	49.14	35.18	15.64	100.31
5	0.36	49.09	35.22	15.59	100.25
6	0.33	49.00	35.15	15.55	100.03
7	0.37	48.95	34.98	15.51	99.81
Mean	0.35	49.09	35.13	15.58	100.14
St. dev.	0.02	0.08	0.11	0.14	0.23
Formula derived: $Ag_{0.04(0)}Pb_{2.91(2)}Bi_{2.07(1)}S_{5.98(2)}$. Simplified formula: $Pb_3Bi_2S_6$					
"Lillianite"*					
1	1.09	47.25	36.14	15.60	100.32
2	0.98	46.76	36.44	15.62	100.03
3	1.05	46.80	36.61	15.70	100.40
4	1.03	46.70	36.45	15.61	100.05
Mean	1.04	46.88	36.41	15.63	100.20
St. dev.	0.04	0.22	0.17	0.04	0.16
Formula derived: $Ag_{0.12(0)}Pb_{2.77(1)}Bi_{2.14(1)}S_{5.98(2)}$. Simplified formula: $Pb_3Bi_2S_6$					
Galena					
1	0.18	85.94	1.07	13.10	100.43
2	0.20	85.59	1.09	13.11	100.10
Cannizzarite					
1	0.17	37.51	44.96	16.25	99.14
Formula derived: $Ag_{0.4}Pb_{45.5}Bi_{53.9}(S,Te)_{127.3}$. Simplified formula: $Pb_{46}Bi_{54}S_{127}$					

* Found to be an oriented, submicroscopic intergrowth of lillianite-related phases, referred to for convenience as "lillianite".
Compositions are expressed in wt%.

Experimental

A small fragment of xilingolite, about $0.025 \times 0.065 \times 0.125$ mm^3 in size, was used for collection of X-ray data on a Siemens SMART CCD system with a flat graphite monochromator using Mo*K*α radiation from a fine-focus sealed tube at 293 K. Approximately a full sphere was measured in reciprocal space up to $2\theta = 56.25°$ (1877 frames, 0.3° rotation width, with an exposure of 60 seconds per frame). Data reduction including intensity integration, background, and Lorentz-polarization corrections, was carried out using the program Saint Plus (Bruker 1997a).

In a first attempt, a monoclinic pseudo-cell with nine-fold *c*-axis was found [*a* 13.511(3), *b* 4.085(1), *c* 185.84(6) Å, β 92.16(2)°]. From systematic absences along the reciprocal axes, it could be shown that this pseudo-cell is the result of twinning. Subsequently, the twin law, cell dimensions, and space group for both individuals could be determined. The measured crystal shows (001) twinning with a twin-domain ratio of about 70:30. In the reciprocal lattice, two *a**–*c** planes are superimposed with a common *c**. Because *c** is perpendicular to (001), both twin individuals have in common the (001) plane, which is interpreted as the twin plane. For one twin domain, the angle between *a** and *c** is 92.16°, and for the other domain, the angle is 87.84°. Exact superposition of reflections between the two twin reciprocal lattices occurs at x*kl* layers for $x = c^*/(2 \cdot a^* \cdot \sin[\beta - 90°])$. This superposition of reflections occurs for xilingolite at x = 8.73. Thus superposition is approximately achieved for 8*kl* and 9*kl* layers and is responsible for the initially observed pseudo-cell

with nine-fold translation parallel to *c*. The refined true unit-cell dimensions are listed in Table 2. They are very similar to those of type xilingolite (Hong *et al.* 1982). Thus we conclude that the crystal under investigation is (001)-twinned xilingolite. With the cell dimensions in Table 2, it was also possible to index the powder pattern published by Graeser in 1984 (Table 3).

Hong *et al.* (1982) reported that xilingolite is not a dimorph of lillianite and that *C*2/*m*, *C*2 or *Cm* are the possible space-groups. The similarity in cell dimensions and cell volume between lillianite and xilingolite suggests two possible structural models for xilingolite. (1) Xilingolite is an (Pb,Bi)-ordered polymorph of $Pb_3Bi_2S_6$, or (2) xilingolite is a different homologous member of the lillianite series with $N_{1,2}$ = 3,5 or 2,6. Geometrical calculations show that model (2) would lead to more pronounced monoclinic distortions than the observed value of β = 92.15°. Thus model (1) was selected for structure refinement. Subsequently, space group *Bbmm* (**bca**) (No. 63) of lillianite was transformed into its standard setting *Cmcm* (**abc**). One of the maximal non-isomorphic subgroups of *Cmcm* is *C*2/*m*11, thus an interchange of **a** and **b** led to the standard monoclinic setting *C*12/*m*1 (or *C*2/*m*, No. 12). This transformation allowed the atom coordinates of lillianite to be calculated in *C*2/*m* symmetry and to be used as a starting model for structure refinement. The nomenclature of atom sites established for lillianite by Takagi & Takéuchi (1972) was extended to xilingolite by adding the suffixes a and b; for example, the site *M*1 in lillianite splits into the symmetry-independent sites *M*1a and *M*1b in xilingolite. Note that direct solution of the structure of a non-merohedral twin is not trivial, and we therefore preferred to test a refinement with an appropriate model. Lack of systematic absences, other than those due to *C*-centering, indicated *C*2/*m* as probable space-group.

For the absorption correction and subsequent refinement of the structure, the initial dataset was reduced. All families of reflections with partial overlap due to twinning were eliminated. Partial overlap of reflections causes problems in reliable integration of intensities and background correction. Therefore, only those families of reflections with total overlap (0*kl*, 8*kl*, 9*kl*) and those without overlap (4*kl*, 5*kl*, 12*kl*, 13*kl*) were used. The latter set of reflection families belongs to one twin domain only. This reduced set of data was used for absorption correction with the pseudo φ-scan technique. One of the major problems in obtaining precise diffraction data of minerals of lillianite homologous series is the strong X-ray absorption of Pb,Bi sulfosalts, even for the short-wavelength Mo*K*α radiation. Xilingolite has a calculated density of 7.185 g/cm^3, leading to a linear absorption coefficient of 76 mm^{-1}. Thus before an empirical correction for absorption, identical reflections measured on multiple frames had R_{INT} = 34%. In spite of the small size of the crystal, the maximum X-ray transmission was only about 5%, and the minimum transmission even one order of magnitude lower. An empirical correction for absorption, applying an elliptical model decreased R_{INT} to 11%. The routine CCD SMART twin utilities could not be applied because these programs do not allow for absorption correction.

TABLE 2. UNIT-CELL PARAMETERS OF XILINGOLITE AND LILLIANITE

	Xilingolite	Xilingolite	Lillianite
Compound	$Pb_3Bi_2S_6$	$Pb_{3+x}Bi_{2-2/3x}S_6$	$Pb_3Bi_2S_6$*
System	monoclinic	monoclinic	orthorhombic
Space group	*C*2/*m*	*C*2/*m*, *C*2 or *Cm*	*Bbmm*
a (Å)	13.511(3)	13.65	13.535(3)
b (Å)	4.0850(11)	4.078	20.451(5)
c (Å)	20.649(2)	20.68	4.104(1)
β (°)	92.15(2)	93.0	
V (Å^3)	1138.9	1149.6	1163.0
Z	4	4	4
Reference	This study	Hong *et al.* (1982)	Takagi & Takéuchi (1972)

* Ignoring weak $Ag^{1+} + Bi^{3+} \leftrightarrow 2\ Pb^{2+}$ substitution.

Structure Refinement

For the structure refinement, the structure model of lillianite (Takagi & Takéuchi 1972) was transformed into the xilingolite unit-cell as indicated above and used as a starting model. For the refinement of the twinned crystal based on $(F_{obs})^2$, we used the program SHELXL97 (Sheldrick 1997) in its HKLF 5 option. With the program XPREP (Bruker 1997b), a *hkl* file was created and subsequently modified in order to characterize each reflection with an additional flag (1 or 2), which determines whether the corresponding reflection originates from the master crystal #1 (*i.e.*, the larger twin-domain,

TABLE 3. X-RAY POWDER-DIFFRACTION DATA FOR XILINGOLITE

h	*k*	*l*	d_{obs}	d_{calc}*	I_{obs}	I_{calc}	*h*	*k*	*l*	d_{obs}	d_{calc}*	I_{obs}	I_{calc}
$\bar{2}$	0	5	3.583	3.585	60	76	1	$\bar{1}$	8	2.145	2.145	60	16
2	0	5	3.468	3.469	50	66	$\bar{6}$	0	4		2.090		15
1	1	3		3.382		42				2.091		70	
			3.373		30		$\bar{5}$	1	4		2.086		20
4	0	0		3.370		32	0	0	10	2.068	2.068	80	15
2	0	6	3.027	3.024	40	13	0	2	0	2.039	2.040	60	33
$\bar{3}$	1	1		3.000		21	$\bar{3}$	1	8	1.9907	1.9900	40	8
			2.981		40		3	1	8	1.9408	1.9406	40	9
3	$\bar{1}$	1		2.978		37				1.7949		40	
$\bar{3}$	1	2	2.915	2.919	50	43				1.7353		40	
3	1	2	2.868	2.879	50	42				1.5150		50	
$\bar{3}$	1	3	2.791	2.792	40	33				1.4693		60	
3	$\bar{1}$	3	2.742	2.742	40	14				1.4542		70	
$\bar{1}$	1	7	2.342	2.344	30	13				1.3504		80	
$\bar{1}$	1	8	2.167	2.167	100	33				1.3222		60	

Notes: 114.6 mm Gandolfi camera, Fe*K*α radiation.
* *d* values calculated for *a* 13.49(1), *b* 4.080(3), *c* 20.71(1) Å, β 92.12(4)° refined from Gandolfi films, G262/264.
I_{obs}: Intensities estimated visually.
I_{calc}: Intensities calculated for the formula $Pb_3Bi_2S_6$ with the program CrystalDiffract (http://www.crystalmaker.co.uk).

flag = 1) or from both twin domains (flag = –2). Isolated families of reflections from crystal #2 (*i.e.*, the smaller twin-domain) were not considered because such reflections were less accurate owing to the lower contribution to the twin (only 30%). Reflections that are influenced by both individuals were grouped into pairs where h_2, k_2, l_2, $(F_{o1})^2$, $\sigma(F_{o1})^2$ from crystal #2 are given first with flag = –2, followed by the indices and $(F_{o1})^2$, $\sigma(F_{o1})^2$ of crystal #1 with flag = 1, and so on. With this coding, the influence of the twin components on the bulk intensity of a reflection (0*kl*, 8*kl*, 9*kl*) was calculated. In addition, the input file of SHELXL97 required a BASF-instruction to refine the contribution of the two twin-components where the calculated value was 1 – (contribution of crystal #1). Additional details pertaining to non-merohedral twin refinements are given by Hoffmann & Armbruster (1995).

According to the above strategy, the structure of (001) twinned xilingolite was refined using scattering factors for neutral atoms. Anisotropic displacement parameters were refined for all atoms in the last cycles. The highest residual peak at the end of the refinement was 2.75 e/Å^3, located 0.07 Å from *M*2b, and the deepest hole, –1.83 e/Å^3, located 1.46 Å from *M*1b. The refinement was stopped when the maximum shift/esd for varied parameters dropped below 0.1. Considering the high R_{INT} = 11%, owing to incomplete correction for anisotropic absorption, the convergence of the refinement at R_1 = 8.65% was satisfying, and other models did not need to be considered. The results of our refinement are represented in Table 4. Fractional coordinates, isotropic and anisotropic displacement parameters of atoms are given in Table 5. Selected interatomic distances and angles are listed in Table 6. Additional material relevant to this paper can be ordered referring to the no. CSD 411957, names of the authors and citation of the paper at the Fachinformationszentrum Karlsruhe, Gesellschaft für wissenschaftlich-technische Information mbH, D–76344 Eggenstein- Leopoldshafen, Germany. The list of F_o/F_c data has been deposited at the Depository of Unpublished Data, CISTI, National Research Council of Canada, Ottawa, Ontario K1A 0S2, Canada.

TABLE 4. SUMMARY OF PARAMETERS DESCRIBING COLLECTION AND REFINEMENT OF CCD DATA FOR XILINGOLITE FROM MITTAL–HOHTENN, SWITZERLAND

X-ray power, Mo$K\alpha$	50 kV, 40 mA, 0.71073 Å
Temperature	293 K
Detector-to-sample distance	5.2 cm
Active detection-area	6.25 × 6.25 cm^2
Resolution	512 × 512 pixels
Sample size	0.025 × 0.065 × 0.125 mm^3
Exposures	1877
Rotation width per frame	0.3°
Measuring time	60 s
Maximum covered 2θ	56.25° (d = 0.75 Å)
Unique reflections	1808
Reflections $I > 2\ \sigma_I$	1520
R_{INT} before absorption correction	34%
R_{INT} after absorption correction	11%
R_σ [$F_o > 4\sigma(F_o)$]	4.26%
Number of least squares parameters	70
Goof	1.072
R_1 [$F_o > 4\sigma(F_o)$]	8.65%
R_1 (all data)	9.54%
wR_2 (on F_o^2)	23.38%

$R_{INT} = \Sigma\ F_o^2 - F_o^2\ (\text{mean}) / \Sigma\ F_o^2$ $\quad R_\sigma = \Sigma\ \sigma(F_o^2) / \Sigma\ F_o^2$

$R_1 = \Sigma\ F_o - F_c / \Sigma\ F_o$ $\quad wR_2 = \sqrt{(\Sigma\ w[F_o^2 - F_c^2]^2 / \Sigma\ w[F_o^2]^2)}$

$\text{Goof} = \sqrt{(\Sigma\ w[F_o^2 - F_c^2] / [n - p])}$ $\quad w = 1 / (\sigma^2[F_o^2] + [0.176 * P]^2)$

$P = (\text{Max}[F_o^2, 0] + 2\ F_c^2) / 3$

Description of the Structure

The crystal structure of xilingolite is shown in Figure 3. It consists of alternating layers of PbS archetype, cut parallel to $(311)_{PbS}$, and each layer is N = 4 octahedra thick. Xilingolite is a $^{4,4}L$ homologue of the lillianite homologous series. The structure contains five symmetry-independent *M* positions occupied by Pb and Bi. The

TABLE 5. XILINGOLITE: FRACTIONAL ATOM COORDINATES, ISOTROPIC AND ANISOTROPIC DISPLACEMENT PARAMETERS (Å^2)*

Atom	*x/a*	*y/b*	*z/c*	U_{iso}	U_{11}	U_{22}	U_{33}	U_{13}
*M*1a	0.09675(12)	0.5	0.13585(9)	0.0381(5)	0.0367(11)	0.0428(9)	0.0347(10)	0.0011(7)
*M*1b	0.91787(13)	0.5	0.63337(8)	0.0399(5)	0.0399(11)	0.0417(10)	0.0380(10)	–0.0013(7)
*M*2a	0.36535(11)	0.5	0.04701(8)	0.0386(6)	0.0367(11)	0.0407(10)	0.0383(10)	0.0005(8)
*M*2b	0.63998(11)	0.5	0.55053(8)	0.0363(5)	0.0340(10)	0.0390(10)	0.0357(9)	–0.0008(7)
*M*3	0.32697(14)	0	0.24043(11)	0.0503(6)	0.0473(12)	0.0456(10)	0.0575(13)	–0.0035(9)
S1a	0.2360(8)	0	0.1007(6)	0.045(3)	0.045(7)	0.047(7)	0.043(7)	–0.003(5)
S1b	0.7651(9)	0	0.5874(7)	0.048(3)	0.044(7)	0.037(6)	0.061(8)	–0.014(6)
S2a	0	0.5	0	0.044(4)	0.048(10)	0.045(9)	0.040(9)	–0.002(7)
S2b	0	0.5	0.5000	0.042(4)	0.033(8)	0.038(8)	0.056(11)	0.007(7)
S3	0.1846(8)	0.5	0.2505(5)	0.036(2)	0.034(6)	0.047(6)	0.027(5)	0.002(4)
S4a	0.4624(9)	0.5	0.1649(6)	0.042(3)	0.045(6)	0.047(6)	0.033(6)	0.004(5)
S4b	0.5569(8)	0.5	0.6648(5)	0.037(2)	0.035(6)	0.047(6)	0.029(5)	0.001(4)

* $U_{12} = U_{23} = 0$.

TABLE 6. SELECTED INTERATOMIC DISTANCES (Å) AND ANGLES (°) FOR XILINGOLITE

*M*1a	S3	S4a	S4a	S1a	S1a	S2a	
S3	2.608(10)	94.7(3)	94.7(3)	87.1(3)	87.1(3)	178.3(2)	
S4a	3.989(14)	2.812(9)	93.2(4)	177.5(3)	88.4(3)	86.5(2)	
S4a	3.989(14)	4.085(1)	2.812(9)	88.4(3)	177.5(3)	86.5(2)	
S1a	3.793(14)	5.699(12)	3.974(17)	2.888(8)	90.0(4)	91.7(2)	
S1a	3.793(14)	3.974(17)	5.699(12)	4.085(1)	2.888(8)	91.7(2)	
S2a	5.658(10)	4.019(11)	4.019(11)	4.262(10)	4.262(10)	3.050(2)	
*M*1b	S3	S4b	S4b	S2b	S1b	S1b	
S3	2.814(11)	98.5(3)	98.5(3)	172.2(2)	85.2(3)	85.2(3)	
S4b	4.278(14)	2.834(8)	92.2(4)	86.9(2)	91.4(3)	174.4(3)	
S4b	4.278(14)	4.085(1)	2.834(8)	86.9(2)	174.4(3)	91.4(3)	
S2b	5.808(11)	4.018(9)	4.018(9)	3.007(2)	89.1(2)	89.1(2)	
S1b	3.958(15)	4.198(16)	5.858(12)	4.235(11)	3.031(9)	84.7(4)	
S1b	3.958(15)	5.858(12)	4.198(16)	4.235(11)	4.085(1)	3.031(9)	
*M*2a	S4a	S2a	S2a	S1a	S1a	S1a	
S4a	2.721(12)	90.7(2)	90.7(2)	86.3(3)	86.3(3)	175.7(3)	
S2a	4.019(11)	2.925(1)	88.6(0)	177.0(2)	91.5(2)	86.3(2)	
S2a	4.019(11)	4.085(1)	2.925(1)	91.5(2)	177.0(2)	86.3(2)	
S1a	3.871(14)	5.856(8)	4.196(11)	2.933(8)	88.3(4)	96.7(3)	
S1a	3.871(14)	4.196(11)	5.856(8)	4.085(1)	2.933(8)	96.7(3)	
S1a	6.013(17)	4.262(10)	4.262(10)	4.661(16)	4.661(16)	3.296(12)	
*M*2b	S4b	S1b	S1b	S2b	S2b	S1b	
S4b	2.651(11)	91.7(3)	91.7(3)	91.6(2)	91.6(2)	178.8(3)	
S1b	3.870(14)	2.741(8)	96.4(5)	174.6(2)	87.9(2)	89.1(4)	
S1b	3.870(14)	4.085(1)	2.741(8)	87.9(2)	174.6(2)	89.1(4)	
S2b	4.018(9)	5.682(9)	3.950(12)	2.948(1)	87.7(0)	87.6(2)	
S2b	4.018(9)	3.950(12)	5.682(9)	4.085(1)	2.948(1)	87.6(2)	
S1b	5.818(18)	4.154(18)	4.154(18)	4.235(11)	4.235(11)	3.167(14)	
*M*3	S3	S3	S1a	S4a	S4a	S4b	S4b
S3	2.819(8)	92.9(4)	79.7(3)	88.7(3)	155.0(3)	79.2(2)	137.6(2)
S3	4.085(1)	2.819(8)	79.7(3)	155.0(3)	88.7(3)	137.6(2)	79.2(2)
S1a	3.793(14)	3.793(14)	3.093(12)	76.1(3)	76.1(3)	137.7(2)	137.7(2)
S4a	4.208(17)	5.865(12)	3.871(14)	3.189(10)	79.7(4)	67.2(2)	115.5(2)
S4a	5.865(12)	4.208(17)	3.871(14)	4.085(1)	3.189(10)	115.5(2)	67.2(2)
S4b	3.847(15)	5.611(10)	5.868(15)	3.536(16)	5.403(11)	3.199(8)	79.4(3)
S4b	5.611(10)	3.847(15)	5.868(15)	5.403(11)	3.536(16)	4.085(1)	3.199(8)

In each block of the table, the distances from the central atom to the ligands are given on the diagonal, the angles between two ligands and the central atom are listed in the upper right corner, and the distances between ligands can be found in the lower left corner.

(010) mirror planes at $y = 0.25$ and 0.75 present in lillianite (*Bbmm* setting) are only approximately obeyed in xilingolite. The major structural difference compared to lillianite is related to *M*3; in lillianite, eight ligands form a bicapped trigonal prism around *M*3 [PbS_{6+2} on the $(010)_{lillianite}$ mirror planes], whereas in xilingolite, seven ligands form a one-sided monocapped trigonal prism (MS_{6+1}). This fact can especially be appreciated if one looks at the corresponding *M*3–S distances. In xilingolite, the capping S atom (S1a, Fig. 3) is at 3.093(12) Å, and the distant S1b is at 3.810(15) Å from *M*3 (average 3.452 Å); in lillianite, the two capping S1 atoms are each at 3.362 Å apart from *M*3.

The remaining four *M* sites are all in slightly distorted octahedral coordination, with *M*–S distances in the range 2.608(10) – 3.296(12) Å (2.638 – 3.273 Å in lillianite). It is important to point out that the mirror-related sites *M*1–*M*1' and *M*2–*M*2' in lillianite give two symmetry-independent positions *M*1a–*M*1b and *M*2a–*M*2b, respectively, in xilingolite. The *M*1a/*M*1–S distances (xilingolite: 2.608(10) – 3.050(2) Å; lillianite 2.687 – 2.993 Å) are similar in the two compounds, but the *M*1b–S distances in xilingolite [2.814(11) – 3.031(9) Å] are clearly longer than those in lillianite. However, the *M*2–S distances in lillianite (2.638 – 3.273 Å) are about halfway between *M*2a–S and *M*2b–S distances in xilingolite [2.721(12) – 3.296(12) Å and 2.651(11) – 3.167(14) Å]. These observations underline the differences in cation order in the two structures (*cf.* Table 7).

If we further assume that the (001) mirror twin-planes occur in xilingolite at $z = 0.25$ or at $z = 0.75$ (or both), twinning transforms b-suffixed positions into a-

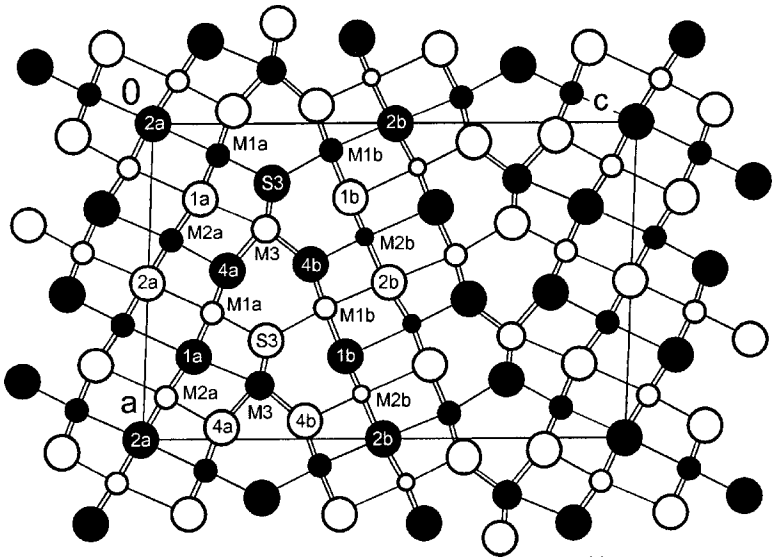

FIG. 3. The crystal structure of xilingolite, $Pb_3Bi_2S_6$, a monoclinic $^{4,4}L$ homologue of the lillianite homologous series. Circles, in order of decreasing size, denote S, Pb, (Pb,Bi), Bi. Void and filled circles indicate atoms at z = 0.5 and 0, respectively, along the 4 Å axis.

suffixed positions (and *vice versa*). Thus twinning mimics true mirror planes observed in lillianite.

DEGREE OF Pb–Bi ORDER

The ions Pb^{2+} and Bi^{3+} are isoelectronic, thus their degree of order cannot be derived from Mo$K\alpha$ X-ray scattering behavior but only from bond lengths (*e.g.*, Hummel & Armbruster 1987, Berlepsch *et al.* 2001). Takagi & Takéuchi (1972) wrote about lillianite that "the coordination and site suggest that *M*3 is occupied by a Pb atom. The differences in bond lengths between *M*1–S and *M*2–S are not significant, suggesting that Pb and Bi atoms are distributed over the two sites at random".

Aizawa *et al.* (1983) used highly idealized strain-energy calculations for so-called chemically twinned phases in the system PbS–Bi_2S_3. They found that for lillianite, Bi on *M*1 and Pb on *M*2 would be preferred in terms of strain energy. However, the authors also noted that any adjustment of cation positions and change in cation distributions would strongly influence the elastic strain energy. Aizawa *et al.* (1983) concluded: "there seems little doubt, therefore, that a cation distribution could be found which would give almost any of these structures minimum elastic strain energies."

Ohsumi (1985) applied synchrotron radiation of wavelength 0.96 Å to study the degree of Pb, Bi order in lillianite and determined, owing to the difference in anomalous dispersion effects of Bi and Pb at this wavelength, that *M*2 contains more Bi than *M*1. This assignment was also confirmed by bond-valence calculations, which indicated 0.54 Pb and 0.46 Bi at *M*1 *versus* 0.54 Bi and 0.46 Pb at *M*2 (Takéuchi 1997), as had been predicted earlier on the basis of the octahedron geometry (Makovicky 1977) expressed in terms of the *l* parameter (Makovicky & Karup-Møller 1977a).

TABLE 7. DEGREE OF ORDER OF Pb AND Bi IN XILINGOLITE AND LILLIANITE, AND BOND-VALENCE SUMS FOR CATIONS IN XILINGOLITE

Xilingolite			Lillianite	
*M*1a	Bi >> Pb	2.85 *vu*	*M*1	Pb ≈ Bi
*M*1b	Pb > Bi	2.21	*M*1′	Pb ≈ Bi
*M*2a	Pb > Bi	2.16	*M*2	Pb ≈ Bi
*M*2b	Bi >> Pb	2.77	*M*2′	Pb ≈ Bi
*M*3	Pb	1.90	*M*3	Pb

M and *M*′ in lillianite are symmetry-related by a mirror plane. *vu*: valence units.

Only $^{4,4}L$ (lillianite) and $^{7,7}L$ (heyrovskyite, aschamalmite) are known in the Ag-free subsystem Pb–Bi–S (Makovicky 1997). A reduction of symmetry in $^{7,7}L$ from the usual orthorhombic to monoclinic, caused by Pb–Bi order over the two mirror-related slabs, was exceptionally observed in aschamalmite: in one slab, a similar Bi-rich pair is observed (Mumme & Makovicky, unpubl. data in Makovicky 1997). An attempt will be made here to evaluate the degree of Pb–Bi order in the structure of xilingolite and lillianite on the basis of element-specific *M*–S bond-length hyperbolae.

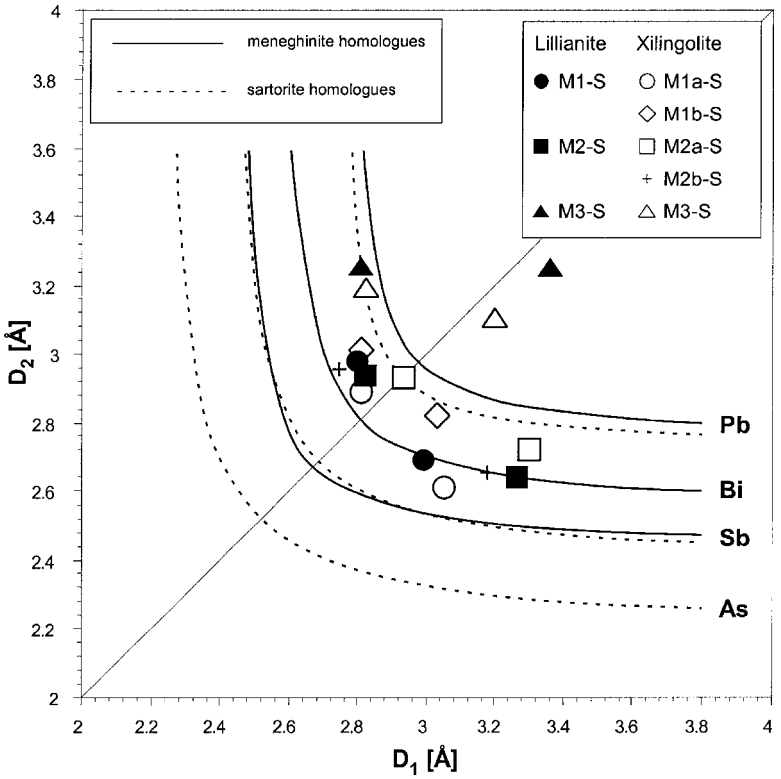

FIG. 4. Element-specific bond-length hyperbolae for pairs of opposing bonds (Berlepsch *et al.* 2001) with individual bond-length data of lillianite and xilingolite added. Each pair of bond lengths consists of a short (x_n) and an opposing long (y_n) *M*–S bond distance (where $x_n < y_n$ and n = 1, 2, 3). $D_1 = x_1, x_2, y_3$ and $D_2 = y_1, y_2, x_3$ define the points P_1 (x_1y_1) ≡ P_2 (x_2y_2) above and P_3 (y_3x_3) below the median line for each coordination polyhedron.

The calculated bond-length hyperbolae in Figure 4 were taken from Berlepsch *et al.* (2001), with the corresponding data for xilingolite and lillianite added. For all but *M*3, the coordination polyhedra around *M* give three pairs of opposing bond-lengths. For each such octahedron, the two pairs of bond lengths in the plane $(001)_{PbS}$ of the galena submotif are identical (*i.e.*, they plot at the same place in the diagram in Fig. 4), but the third one along $[001]_{PbS}$ of the galena submotif is different. By our own convention, the former pair of bond lengths is drawn above, and the latter pair below the median line in Figure 4. The definition of pairs of bond lengths in *M*3 coordination polyhedra is only tentative since they are not octahedra but mono- and bicapped trigonal prisms, respectively. Only the pairs of bond lengths that lie in the extension of the $(001)_{PbS}$ planes from the adjacent slabs follow the hyperbolic relationship; the other does not (Fig. 4).

The plot in Figure 4 confirms the interpretation of Takagi & Takéuchi (1972), who interpreted *M*3 as a Pb position and *M*1 and *M*2 as mixed (Pb,Bi) positions in lillianite. The *M*3 pairs of bond lengths above the median line plot on the Pb hyperbola, whereas *M*1 and *M*2 pairs of bond lengths above the median line plot between the hyperbolae for Pb and Bi. For the pairs of bond lengths below the median line, the situation resembles bismuth more closely, suggesting perhaps that the element with the more active lone-electron pair, *i.e.*, Bi, has more influence on the bond-length ratios in the direction perpendicular to the slab thickness, in which the lone-electron pair micelles (*i.e.*, the interspaces that accommodate lone-electron pairs of quasi-octahedral Pb and Bi) can find their best expression.

For xilingolite, the situation is very similar in the case of *M*3; we interpret it as a Pb position. On the contrary, *M*2b seems to be occupied by Bi only. For the

remaining three mixed *M* sites, a preference of Bi is suggested for *M*1a, whereas Pb dominates over Bi at *M*2a and *M*1b. The interpretations are summarized in Table 7. We applied the bond-valence approach (Brown & Altermatt 1985) with a common r_0 parameter of 2.543 for Bi^{3+} and Pb^{2+} (Hummel & Armbruster 1987); the calculated valence-sums (Table 7) all plot in the histograms either characteristic of pure Bi^{3+} or pure Pb^{2+} sites (Fig. 2a of Hummel & Armbruster 1987). Thus even complete Pb, Bi order in xilingolite cannot be excluded. The conclusion is that Pb and Bi show a higher degree of order in xilingolite, which is responsible for the reduction in symmetry compared to that of lillianite.

Discussion

The pattern of order is opposite in the two sets of slabs, disordered (Pb, Bi) in *M*1 separating into ~Bi in *M*1a in slab "a" and into ~Pb in *M*1b in slab "b". The *M*2 speciation goes the opposite way, *M*2a being primarily Pb in slab "a", and *M*2b being heavily Bi in slab "b".

The "opposite" scheme is probably the only way to order the atoms involved: *M*1a and *M*1b as well as *M*2a and *M*2b compensate mutually their requirements; the smaller polyhedra alternate with larger polyhedra in the $(001)_{PbS}$ and $(111)_{PbS}$ planes, as well as in the $[001]_{xilingolite}$ direction. The lone-electron-pair micelle of *M*1a and *M*2a is more strongly expressed *via* longer *M*1a–S2a and *M*2a–S1a distances than that in slab "b"; slab "b" seems to be closer to a regular PbS-like arrangement.

The definite preference of Bi^{3+} for *M*2b can be connected with the monocapped trigonal prismatic coordination of *M*3 (Pb) in xilingolite. Because S1b does not participate in *M*3 bonding (in contrast to lillianite), S1b becomes bond-strength-undersaturated. S1b bonds only to *M*1b and *M*2b; thus Bi^{3+} in *M*2b attaches itself with two strong bonds, in order to balance the underbonding of S1b. The S2a is not without problems either: it has two long distances *M*1a–S2a and four bonds *M*2a–S2a of average Pb–S length. S1a is not overbonded either: the *M*3–S1a bond is clearly very long, and *M*2a–S1a is an average Pb–S bond as well. It might therefore attract *M*1a = Bi as a neighbor. It might win competition for the *M*3–S bond; unlike S1b, which is satisfied by the short *M*2b–S1b bonds, *M*1a–S1a are not the shortest bonds.

The above arguments probably have to be reversed from the viewpoint of crystal growth: an ordered arrangement of Bi^{3+} at *M*2b leads to overbonding of S1b. Thus S1b cannot complete the bicapped trigonal prismatic coordination of *M*3 as observed for lillianite. For this reason, *M*3 in xilingolite has only monocapped trigonal prismatic coordination and monoclinic *C*2/*m* symmetry. The "opposite" order might provide a better overall packing scheme at the time of growth, with *M*3 flipping as a consequence of it.

Why is beta as it is? The start of the determining process might be the order at *M*1a (Bi) *versus* *M*1b (Pb). Pb at *M*1b has a larger polyhedron (33.1 Å^3; *M*1a = 30.5 Å^3), leading to a small shift of S4b and also S2b in –**a** direction compared to S4a and S2a. Furthermore, the *M*3 monocapped trigonal prism (40.1 Å^3) will lose its bilateral symmetry, and S4b will "rotate" upward (*i.e.*, in the direction of –**a**) to be more in line with the monocapped shape. This rotation is helped by the larger dimensions [in the (010) plane] of the *M*2a octahedron (3.296 + 2.721 Å; 34.2 Å^3) compared to the *M*2b polyhedron (2.651 + 3.167 Å; 31.3 Å^3).

Several sulfides exhibit crystal-chemical features akin to those of xilingolite. First of all, aschamalmite (Mumme *et al.* 1983), idealized as $Pb_6Bi_2S_9$, displays both order of Pb and Bi over the octahedral sites and the asymmetric position of the trigonal prismatic coordination polyhedron containing the lead atom. The asymmetric position is also assumed by the trigonal prismatic Y^{2+} site in $Y^{2+}Y^{3+}{}_4S_7$ (Adolphe 1965), an N = 1,2 lillianite structure. Other related structures are the synthetic pavonite homologue N = 6, $CuPb_3Bi_5Se_{11}$ (Mumme 1990), and the V phases in the $PbS–Bi_2S_3$ system (Takéuchi *et al.* 1974, 1979). The asymmetric trigonal prismatic site is occupied by Pb in the former structure and by the (Pb,Bi) mixture in the V phases. In all these phases, the short bond between the cation and the prism cap ligand is oriented toward (or, is part of) the thinner PbS-like slab, which has N = 1 for all cases. Therefore, with both slabs of the same and considerable thickness, the ordering process in xilingolite and aschamalmite is in some respects unique among complex sulfides.

Our structure determination of xilingolite is the first substantial contribution to the problem of cation ordering in lillianite homologues with N = 4,4. It is paralleled to certain extent by a sister work on aschamalmite (Mumme *et al.* 1983, Mumme & Makovicky, in prep.). Before these studies, only the orthorhombic N = 4,4 and 7,7 forms were known and analyzed, on the basis of a disordered distribution of Pb and Bi over equivalent sites. Future work should comprise detailed chemical studies in order to determine the cations present in coexisting lillianite homologues with ordered and disordered distribution of cations, respectively, and with studies aimed at determining whether the ordered derivatives crystallized directly from solutions or formed as a result of slow ordering of originally disordered crystals in the solid state.

Acknowledgements

We are grateful to H.-R. Rüegg, who brought the mysterious mineral M2 to our attention. The constructive reviews and valuable suggestions of two anonymous referees are greatly acknowledged. We thank Associate Editor F. Vurro (Bari, Italy) for the rapid handling of this paper and Robert F. Martin for linguistic

improvements to the text. Additional help by F. Vurro, M. Nespolo (Ibaraki, Japan), and Robert F. Martin is highly appreciated.

References

ADOLPHE, C. (1965): Contribution a l'étude d'un groupe de sulfures isostructuraux de terres rares et d'yttrium de type: Y_5S_7 et FeY_4S_7. *Ann. Chim.* **10**, 271-297.

AIZAWA, K., IGUCHI, I. & TILLEY, R.J.D. (1983): The elastic strain energy and stability of some idealized lead–bismuth sulphides. *J. Solid State Chem.* **48**, 284-294.

BERLEPSCH, P., MAKOVICKY, E. & BALIĆ-ŽUNIĆ, T. (2001): The crystal chemistry of meneghinite homologues and related compounds. *Neues Jahrb. Mineral., Monatsh*., 115-135.

BROWN, I.D. & ALTERMATT, D. (1985) : Bond valence parameters obtained from a systematic analysis of the inorganic crystal structure database. *Acta Crystallogr.* **B41**, 244-247.

BRUKER (1997a): SAINT PLUS, Version 6.02/NT– Bruker Analytical X-ray Systems.

_____ (1997b): XPREP, Version 5.1/NT. Data preparation and reciprocal space exploration. Bruker Analytical X-ray Systems.

GRAESER, S. (1971): Mineralogisch-geochemische Untersuchungen an Bleiglanz und Zinkblende. *Schweiz. Mineral. Petrogr. Mitt.* **51**, 415-442.

_____ (1984): Die Mineralien des Strassentunnels Mittal-Hohtenn/VS. *Schweizer Strahler* **12**(6), 293-309.

HOFFMANN, C. & ARMBRUSTER, T. (1995): Crystal structure of a (001) twinned sussexite $Mn_2B_2O_4(OH)_2$ from the Kalahari Manganese Field, South Africa. *Schweiz. Mineral. Petrogr. Mitt.* **75**, 123-133.

HONG HUIDI, WANG XIANGWEN, SHI NICHENG & PENG ZHIZHONG (1982): Xilingolite, a new sulfide of lead and bismuth, $Pb_{3+x}Bi_{2-2/3x}S6$. *Acta Petrol. Mineral. Anal.* **1**, 14-18 (in Chinese, with English abstr.).

HUMMEL, W. & ARMBRUSTER, T. (1987): Tl^+, Pb^{2+}, and Bi^{3+} bonding and ordering in sulphides and sulphosalts. *Schweiz. Mineral. Petrogr. Mitt.* **67**, 213-218.

MAKOVICKY, E. (1977): Chemistry and crystallography of the lillianite homologous series. III. Crystal chemistry of lillianite homologues. Related phases. *Neues Jahrb. Mineral., Abh.* **131**, 187-207.

_____ (1997): Modular crystal chemistry of sulphosalts and other complex sulphides. *In* Modular Aspects of Minerals (S. Merlino, ed.) *Eur. Mineral. Union, Notes in Mineralogy* **1**, 237-271.

MAKOVICKY, M. & KARUP-MØLLER, S. (1977a): Chemistry and crystallography of the lillianite homologous series. I. General properties and definitions. *Neues Jahrb. Mineral., Abh.* **130**, 264-287.

_____ & _____ (1977b): Chemistry and crystallography of the lillianite homologous series. II. Definition of new minerals: eskimoite, vikingite, ourayite and treasurite. Redefinition of schirmerite and new data on the lillianite–gustavite solid solution series. *Neues Jahrb. Mineral., Abh.* **131**, 56-82.

MUMME, W.G. (1990): A note on the occurrence, composition and crystal structures of the pavonite homologous series ^{4}P, ^{6}P, and ^{8}P. *Neues Jahrb. Mineral., Monatsh.*, 193-204.

_____, NIEDERMAYR, G., KELLY, P.R. & PAAR, W.H. (1983): Aschamalmite, $Pb_{5.92}Bi_{2.06}S_9$, from Untersulzbach valley in Salzburg, Austria – "monoclinic heyrovskyite", *Neues Jahrb. Mineral., Monatsh.*, 433-444.

OHSUMI, K. (1985): Determination of site occupancies of atoms with neighbouring atomic numbers. *Nippon Kessho Gakkaishi* **27**, 73-80 (in Japanese).

SHELDRICK, G.M. (1997): *SHELXL97, Release 97–1, Computer Program for Crystal Structure Refinement*. University of Göttingen, Göttingen, Germany.

SWIDERSKI, B. (1919): Carte géologique de la partie occidentale du Massif de l'Aar. *Commission géologique de la Société helvétique des Sciences naturelles (Berne), Carte spéciale* **89**.

TAKAGI, J. & TAKÉUCHI, Y. (1972): The crystal structure of lillianite. *Acta Crystallogr.* **B28**, 649-651.

TAKÉUCHI, Y. (1997): Homologous series in the PbS–Bi_2S_3 system and extended lillianite homologous series. *In* Tropochemical Cell-twinning, a Structure-Building Mechanism in Crystalline Solids. *Terra Scientific Publishing Company*, Tokyo, Japan (15-34).

_____, OZAWA, T. & TAKAGI, J. (1979): Tropochemical cell-twinning and the 60 Å structure of phase V in the PbS–Bi_2S_3 system. *Z. Kristallogr.* **150**, 75-84.

_____, TAKAGI, J. & YAMANAKA, T. (1974): Structural characterization of the high-temperature phase V on the PbS–Bi_2S_3 join. *Z. Kristallogr.* **140**, 249-272.

Received July 1, 2001, revised manuscript accepted October 16, 2001.